



HAL
open science

Cysteine scanning mutagenesis and disulfide mapping analysis of arrangement of GspC and GspD protomers within the type 2 secretion system

X. Wang, C. Pineau, S. Gu, N. Guschinskaya, R. W. Pickersgill, V. E. Shevchik

► To cite this version:

X. Wang, C. Pineau, S. Gu, N. Guschinskaya, R. W. Pickersgill, et al.. Cysteine scanning mutagenesis and disulfide mapping analysis of arrangement of GspC and GspD protomers within the type 2 secretion system. *Journal of Biological Chemistry*, 2012, 287 (23), pp.19082-93. 10.1074/jbc.M112.346338 . hal-02001294

HAL Id: hal-02001294

<https://hal.science/hal-02001294>

Submitted on 27 May 2021

HAL is a multi-disciplinary open access archive for the deposit and dissemination of scientific research documents, whether they are published or not. The documents may come from teaching and research institutions in France or abroad, or from public or private research centers.

L'archive ouverte pluridisciplinaire **HAL**, est destinée au dépôt et à la diffusion de documents scientifiques de niveau recherche, publiés ou non, émanant des établissements d'enseignement et de recherche français ou étrangers, des laboratoires publics ou privés.



Distributed under a Creative Commons Attribution 4.0 International License

Cysteine Scanning Mutagenesis and Disulfide Mapping Analysis of Arrangement of GspC and GspD Protomers within the Type 2 Secretion System^{*[S]}

Received for publication, January 25, 2012, and in revised form, March 28, 2012. Published, JBC Papers in Press, April 20, 2012, DOI 10.1074/jbc.M112.346338

Xiaohui Wang[‡], Camille Pineau[‡], Shuang Gu[§], Natalia Guschinskaya[‡], Richard W. Pickersgill^{§1}, and Vladimir E. Shevchik^{‡2}

From the [‡]Université de Lyon, F-69003, Université Lyon 1, INSA-Lyon, Villeurbanne F-69621, CNRS, UMR5240, Microbiologie Adaptation et Pathogénie, Lyon F-69622, France and the [§]School of Biological and Chemical Sciences, Queen Mary University of London, London E1 4NS, United Kingdom

Background: The type II secretion system is a multiprotein complex spanning both membranes of Gram-negative bacteria.

Results: We studied organization of the GspC and GspD subunits and map their interaction sites within the functional machinery.

Conclusion: GspC and GspD subunits are organized in a dynamic network, involving multiple transient interactions.

Significance: These findings are crucial to understand the mechanism of this secretion machinery.

The type II secretion system (T2SS) secretes enzymes and toxins across the outer membrane of Gram-negative bacteria. The precise assembly of T2SS, which consists of at least 12 core-components called Gsp, remains unclear. The outer membrane secretin, GspD, forms the channels, through which folded proteins are secreted, and interacts with the inner membrane component, GspC. The periplasmic regions of GspC and GspD consist of several structural domains, HR^{GspC} and PDZ^{GspC}, and N0^{GspD} to N3^{GspD}, respectively, and recent structural and functional studies have proposed several interaction sites between these domains. We used cysteine mutagenesis and disulfide bonding analysis to investigate the organization of GspC and GspD protomers and to map their interaction sites within the secretion machinery of the plant pathogen *Dickeya dadantii*. At least three distinct GspC-GspD interactions were detected, and they involve two sites in HR^{GspC}, two in N0^{GspD}, and one in N2^{GspD}. None of these interactions occurs through static interfaces because the same sites are also involved in self-interactions with equivalent neighboring domains. Disulfide self-bonding of critical interaction sites halts secretion, indicating the transient nature of these interactions. The secretion substrate diminishes certain interactions and provokes an important rearrangement of the HR^{GspC} structure. The T2SS components OutE/L/M affect various interaction sites differently, reinforcing some but diminishing the others, suggesting a possible switching mechanism of these interactions during secretion. Disulfide mapping shows that the organization of

GspD and GspC subunits within the T2SS could be compatible with a hexamer of dimers arrangement rather than an organization with 12-fold rotational symmetry.

The transport of proteins and nucleoprotein complexes across the two membranes of the Gram-negative bacteria requires specialized secretion machineries. The type II secretion system (T2SS)³ is widely employed by pathogenic Gram-negative bacteria to secrete toxins and lytic enzymes facilitating host invasion (1, 2). The plant pathogen *Dickeya dadantii* (ex *Erwinia chrysanthemi*) uses this system, called Out, to secrete several cell wall-degrading enzymes. Dependent on bacteria, the T2SS consists of 12–15 proteins, generally called GspA to GspO and GspS, and certain of them constitute large oligomeric assemblies. The T2SS spans the two bacterial membranes and ensures secretion of folded proteins across the outer membrane pore formed by GspD. GspC, GspL, GspM, and GspF constitute together the inner membrane complex (3–6). The cytoplasmic domains of GspL and GspF interact with an ATPase, GspE. GspE is thought to energize the formation of a short pseudopilus by several pilin-like proteins, GspG to GspK. This pseudopilus probably pushes the proteins through the outer membrane pore, constituted by GspD. The opening of this pore would need to be tightly regulated to allow for an efficient secretion of large folded proteins but, at the same time, prevent any leakage of the periplasmic constituents. GspD and GspC possess large periplasmic regions that are thought to interact and to be involved in the recognition of the secretion substrate (7–10).

The secretin GspD is the unique outer membrane core component of the T2SS (1, 11). In some T2SSs, an outer membrane lipoprotein, pilotin GspS, ensures proper targeting and assembly of the cognate secretin (12–14). Secretins are also involved

* This work was supported by the CNRS, a grant from French ANR-2010-BLANC-1531 SecPath program and LyonBioPole, the Biotechnology and Biological Sciences Research Council, Higher Education Funding Council for England, and Queen Mary University of London.

[S] This article contains supplemental Tables S1 and S2, Figs. S1–S7, and text.
¹ To whom correspondence may be addressed. Tel.: 44-0-20-7882-8444; Fax: 44-0-20-7882-7732; E-mail: r.w.pickersgill@qmul.ac.uk.

² To whom correspondence may be addressed: Université de Lyon, Bat. Lwoff, 10, rue R. Dubois, Villeurbanne, F-69622, France. Tel.: 33-0-4-72-44-58-27; Fax: 33-0-4-72-43-15-84; E-mail: vladimir.shevchik@insa-lyon.fr.

³ The abbreviations used are: T2SS, type II secretion system; ETEC, enterotoxigenic *Escherichia coli*; HR, homology region; PDB, Protein Data Bank; T4P, type IV pili.

TABLE 1
Bacterial strains and plasmids used in this study

Strain	Genotype/phenotype	Reference
<i>Escherichia coli</i> NM522	<i>supE thi-1 Δ (lac-proAB)Δ (mcrB-hsdSM)5 (r_K⁻ m_K⁺)</i> [F' <i>proAB lac^qZΔM15</i>]	Stratagene
<i>Dickeya dadantii</i>		
A350	<i>rafR ganB</i>	(42)
A3556	<i>rafR ganB ΔoutC</i>	(9)
A3558	<i>rafR ganB ΔoutD</i>	(9)
A5274	<i>rafR ganB outC</i> (V143C)	This work
A5176	<i>rafR ganB outC</i> (V144C)	This work
A5177	<i>rafR ganB outC</i> (L145C)	This work
A5211	<i>rafR ganB outC</i> (V153C)	This work
A5212	<i>rafR ganB outC</i> (L154C)	This work
Plasmids		
pTdB-oC ^a	pT7-6 carrying <i>outC</i> under <i>PpelC</i>	(9)
pTdB-oD ^a	pT7-6 carrying <i>outD</i> under <i>PpelC</i>	(24)
pTdB-oCoD ^a	pT7-6 co-expressing <i>outC</i> and <i>outD</i> under <i>PpelC</i>	This work
pTDLB-oCoD ^a	pT7-6 carrying <i>pelB</i> followed by <i>outC</i> and <i>outD</i> under <i>PpelC</i>	This work
pACT3	Cloning vector, p15A <i>ori</i> , the <i>tac</i> promoter, Cm ^R	(43)
pACT3-oS	pACT3 carrying <i>outs</i> under <i>Ptac</i>	This work
pACYC184	Cloning vector, p15A <i>ori</i> , Tc ^R , Cm ^R	(44)
pACPLB	pACYC184 carrying <i>pelB</i>	(24)
pBADIK	Cloning vector, pBAD24 derivative, K _m ^R	(45)
pK-ELM	pBADIK co-expressing HA-OutE, VSV-OutL and cMyc-OutM	B. Py

^a Plasmids expressing cysteine variants of OutC and OutD are listed in supplemental Table S1.

in certain other transport machineries, namely the type III secretion system (T3SS), type IV pili (T4P) and the filamentous phage assembly (15–18). Secretins form pore-like toroidal structures composed of 12–14 protomers, through which secretion substrates can be translocated (16, 18–21). The pore-forming activity has been attributed to the conserved C-terminal portion of secretins, whereas their variable N-terminal part is thought to span the periplasm and to be involved in the recognition of the secretion substrate (9, 22–25). In the secretin GspD, this region consists of four domains, N0–N3. The recently elucidated crystal structure of the N0–N1–N2 domains from ETEC revealed their structural homology with several domains from certain other bacterial and phage machineries (26–28). Specifically, the N0 domain is found in secretins from T2SS, T3SS, and T4P and is structurally similar to certain domains from T4SS, T6SS, and from a TonB-dependent receptor FpvA (18). The N1 and N2 domains both exhibit a similar KH-like fold and show a significant structural homology with several ring-forming proteins from T3SS. The four periplasmic domains of GspD together form a vestibule-like structure, in which the secretion substrate could be loaded prior to being secreted (20, 25).

GspC is an inner membrane protein consisting of a short N-terminal cytoplasmic sequence and an α -helical transmembrane segment, followed by two periplasmic domains: a so-called homology region (HR) and a C-terminal PDZ domain (29, 30). The transmembrane segment of OutC drives the protein oligomerization (31). The PDZ domain seems to be involved in the recognition of certain secretion substrates (9), but it may be substituted by a coiled-coil domain or it may even be absent in some GspCs (30). The structural analysis supposed that the PDZ domain of GspC could exhibit a particular mode of substrate recognition (7). The structure of the HR domain from *Escherichia coli* and *D. dadantii* has recently been elucidated and revealed a β -sandwich fold consisting of two β -sheets each composed of three anti-parallel β -strands (32,

33). HR was shown to interact with the periplasmic region of GspD (7, 8), but the molecular mechanisms of this interaction remain elusive. Truncation analysis, combined with pulldown assays, revealed that a short segment of HR, consisting of strands $\beta 6^{\text{HR}}$ and $\beta 7^{\text{HR}}$, interacts with two distinct sites of GspD, one located in the N0 domain and another in the N2–N3 domains (8). Recent structural studies have addressed this question by crystallographic and NMR analysis, and they indicate another mode of interaction. Both the crystal and the solution HR/N0 interfaces involve strand $\beta 1^{\text{HR}}$ of HR but with two different sites in N0, strands $\beta 1^{\text{N0}}$ and $\beta 3^{\text{N0}}$, respectively (32, 33).

In this study, we have exploited these recent structural data and used cysteine mutagenesis and *in vivo* disulfide bonding analysis to map the interactions between the HR domain of OutC (GspC) and the periplasmic region of OutD (GspD) in their native environment, namely the T2SS of the plant pathogen *D. dadantii*. We have found at least three relevant sites of interaction, we have demonstrated that some other T2SS components and the secreted proteins affect these interactions, and we have revealed some important features of organization of the GspD and GspC protomers within the secretion machinery.

EXPERIMENTAL PROCEDURES

Strains, Plasmids, and Growth Conditions—The bacterial strains and plasmids used in this study are listed in Table 1 and supplemental Table S1. The bacteria were usually grown in Luria-Bertani (LB) medium at 30 °C with shaking at 150 rpm. When required, antibiotics were used at the following final concentrations: 50 $\mu\text{g/ml}$ chloramphenicol, 150 $\mu\text{g/ml}$ ampicillin, 100 $\mu\text{g/ml}$ kanamycin.

DNA cloning and manipulation were carried out using standard methods. Site-directed mutagenesis was performed with the QuikChange kit (Stratagene) and the primers listed in supplemental Table S2. The sequences of mutant genes were all checked (Eurofins MWG Operon). Plasmids pTdB-oC and

GspC-GspD Disulfide Bonding Analysis

pTdB-oD, expressing *outC* or *outD* genes, respectively, under the control of *PpelC*, were constructed earlier (9, 24). The pTdB-oCoD plasmid, co-expressing *outC* and *outD* genes, was constructed by cloning the corresponding DNA fragment under the control of *PpelC*. To co-express the pectate lyase PelB with *outC* and *outD*, *pelB* was cloned upstream of *PpelC*, thus creating pTPLB-oCoD.

D. dadantii mutant strains, carrying chromosomal mutant *outC* alleles that code for cysteine variants, were constructed by marker exchange- eviction mutagenesis, as described previously (9). Briefly, the *D. dadantii* A2365 strain, sucrose-sensitive and secretion-deficient because it carries the *nptI-sacB-sacR* (Km^R) cartridge into the chromosomal *outC*, was transformed with a pTdB-oC plasmid bearing the required mutant *outC* gene. Then, the mutant allele was exchanged for the chromosomal allele by selecting for sucrose tolerance and sensitivity to kanamycin. A correct recombination of the *outC* mutant alleles into the chromosome was systematically checked by PCR using OuC and ROuC primers (supplemental Table S2).

Functional Tests and in Vivo Disulfide Cross-linking Analysis—To assess the functional relevance of single cysteine substitutions in OutC and OutD, each mutant allele was introduced into either a pTdB-oC or a pTdB-oD plasmid and expressed in *D. dadantii* $\Delta outC$ or $\Delta outD$ mutant strain, respectively. The level of pectinase secretion, which reflects the functionality of the respective variants, was assessed by immunoblotting with anti-PelD and anti-PelI antibodies, as described (31).

To assess the extent of disulfide cross-linking, the spontaneous formation of disulfide bonds in steady-state cultures was examined. We considered that the oxidative environment of the periplasm is adequate for generating disulfide bonds between proximal residues during bacterial growth. Preliminary experiments showed that induction of disulfide bonding by the addition of an external oxidant, copper phenanthroline, increased the extent of cross-linking but drastically reduced its specificity (data not shown). Briefly, bacteria were grown overnight at 30 °C in LB supplemented, if necessary, with 1 mM isopropyl 1-thio- β -D-galactopyranoside, 0.3 mg/ml arabinose, and appropriate antibiotics. Cells from 1 ml of culture (A_{600} of 2.0) were spun at 10,000 $\times g$ for 1 min and washed with TBS (50 mM Tris-HCl, pH 7.5, 100 mM NaCl). Next, to block the free thiol groups and prevent further disulfide bond formation, the cells were incubated in the same volume of 20 mM iodoacetamide in TBS for an additional 30 min at 25 °C. The cells were then pelleted, resuspended in 200 μ l of Laemmli sample buffer, without 2-mercaptoethanol, and lysed in boiling water for 10 min. The samples were subsequently incubated for 15 min at 30 °C with benzonase (Sigma-Aldrich), separated using 10% SDS-PAGE, and then analyzed by immunoblotting with anti-OutC and anti-OutD antibodies, as described previously (9, 24).

Molecular Modeling—The N-terminal part of OutD (residues 28–262) was modeled with the homology molecular modeling program MODELLER 9v10 (34). The software identified the following two crystal structures as templates, allowing a confident modeling of the studied region: PDB ID 3EZJ (N-terminal domain of the secretin GspD from *E. coli* ETEC H10407) and PDB ID 3OSS (GspC-GspD complex from the type II secre-

tion system of *E. coli* ETEC H10407). Twenty distinct models have been generated, and their geometry was assessed by a Ramachandran plot calculated with the program PROCHECK (35). The most satisfying model was then retained. It has 92.4% of nonproline and nonglycine residues in the most favored regions, 7.6% in additionally allowed regions, and none in disallowed regions.

RESULTS

Experimental Strategy of Cysteine Scanning Mutagenesis of OutC and OutD—OutD and the periplasmic region of OutC are naturally lacking cysteines. The only endogenous Cys-27 is located in the transmembrane segment of OutC and does not form disulfide bonds *in vivo* (31). Therefore, we first introduced single cysteine substitutions into several selected sites of OutC and OutD and assessed the functionality and disulfide cross-linking pattern of each of these single variants in *D. dadantii* $\Delta outC$ and $\Delta outD$ strains, respectively. Then, combinations of OutC and OutD variants were co-expressed, and the extent of disulfide cross-linking between them was systematically assessed to estimate the proximity of the corresponding sites. Based on previous studies, we restricted this analysis to certain positions selected in the HR domain of OutC and the N0, N2, and N3 domains of OutD. Notably, recent structural studies have indicated that the HR/N0 interface involves strand $\beta 1^{HR}$ and could include either strand $\beta 1^{N0}$ or $\beta 3^{N0}$ (32, 33). Thus, some residues involved in these putative interfaces were examined, namely Gly-99 and Val-100 ($\beta 1^{HR}$), Ser-33 and Phe-34 ($\beta 1^{N0}$), and Ile-64 and Ser-65 ($\beta 3^{N0}$) (Fig. 1). In a previous *in vitro* study (8), the OutC-OutD interaction sites had been mapped to a short segment of the HR domain, consisting of strands $\beta 6^{HR}$ and $\beta 7^{HR}$, and to two distant, but less definite sites of OutD, involving the N0 and N2-N3 domains, respectively (8). To examine this site of HR, cysteines were introduced into the $\beta 6^{HR}$ and $\beta 7^{HR}$ strands to replace Val-143, Val-144, Leu-145, Tyr-151, Val-153, and Leu-154 (Fig. 1). Because the HR domain and the presumed structural HR/N0 interfaces are composed exclusively of β -strands, a plausible mode of HR-OutD interactions could be the “ β -strand addition” mechanism (36). The N0, N1, and N2 domains have mixed α/β -folds, and several β -strands could be potentially involved in such interactions. Consequently, in addition to the OutD variants mentioned above, several residues located in strands $\beta 2^{N0}$ (Thr-53, Val-54, Ile-55, and Ile-56), $\beta 10^{N2}$ (Val-232), $\beta 11^{N2}$ (Val-241) and in the presumed strand $\beta 12^{N3}$ (Val-271 and Ile-272) were selected for this study (Fig. 1). Strand $\beta 2^{N0}$ was investigated in particular because it was thought to bind an extra β -strand from another protein (26).

Periplasmic Domains of OutD Form Homodimers—To examine the relevance of the selected cysteine substitutions in OutD, the corresponding variants were expressed in the *D. dadantii* $\Delta outD$ A3558 strain. Although all of these OutD variants were produced at the wild-type level (Fig. 2B, lower), some of them were fully or partially defective in secretion. More precisely, secretion was fully arrested with F34C, T53C, I55C, I64C, and V232C variants and partially impaired with S33C, S65C, V241C, and G190C, but it was at the wild-type level with the other cysteine variants (Fig. 2A). Nonreducing gels revealed a

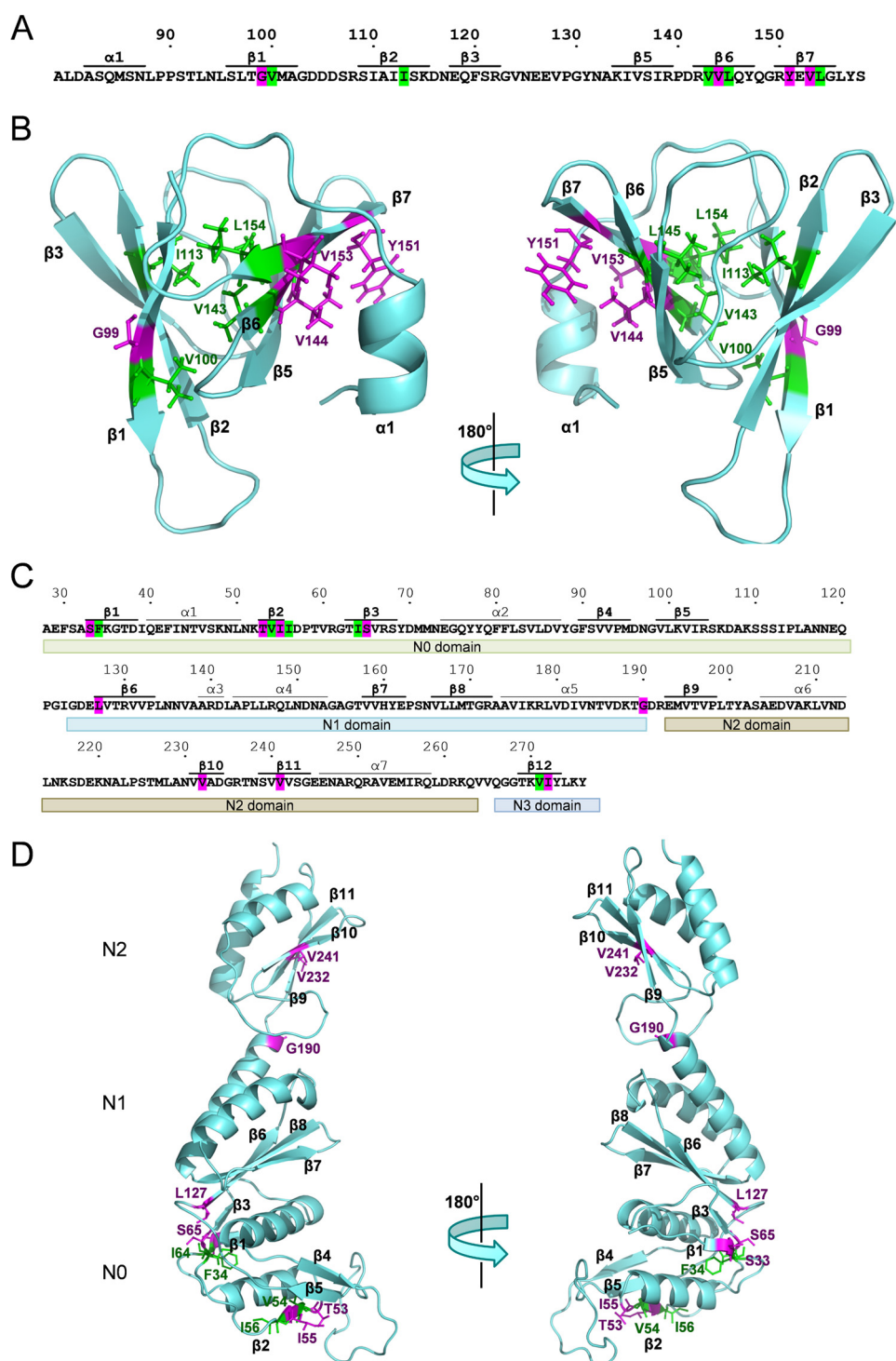


FIGURE 1. Overview of the positions in OutC and OutD selected for cysteine mutagenesis. A and C, sequence of the HR domain of OutC (A) and of N0-N1-N2 domains of OutD (C) from *D. dadantii*, with positions of secondary structure elements. The positions of the cysteine substitutions analyzed in this study are highlighted. B and D, structure of the HR domain of OutC (B) and of the N0-N1-N2 domains of OutD (D). The residues supplemented with cysteine are represented as sticks. B and D were produced using PyMOL. The HR structure is from Ref. 33 (PDB 2LNV), and the N-terminal part of OutD (residues 28–262) was modeled with the homology molecular modeling program MODELLER 9v10 (34) by using the structure of peri-GspD from ETEC as template (PDB ID 3EZJ and 3OSS) (26, 32). The solvent-exposed side chains are shown in magenta, and the buried ones are in green. To visualize the substituted residues more clearly, the structures were rotated around the y axis by 180°.

variable quantity of homodimers with the tested OutD variants, except for L127C, V271C, and I272C which remained monomeric (Fig. 2B). Consistent with the structural data, cysteine substitutions of residues with solvent-exposed side chains, e.g. Thr-53 and Ile-55 (strand $\beta 2^{\text{N0}}$), generated a far greater quan-

tity of dimers than those of the adjacent, but buried, residues Val-54 and Ile-56 (Fig. 2B, compare lanes 5 and 7 with 6). Consistent with the contrasting cross-linking patterns, the latter two OutD variants were functional whereas T53C and I55C were completely defective in secretion (Fig. 2A, lanes 7–10).

GspC-GspD Disulfide Bonding Analysis

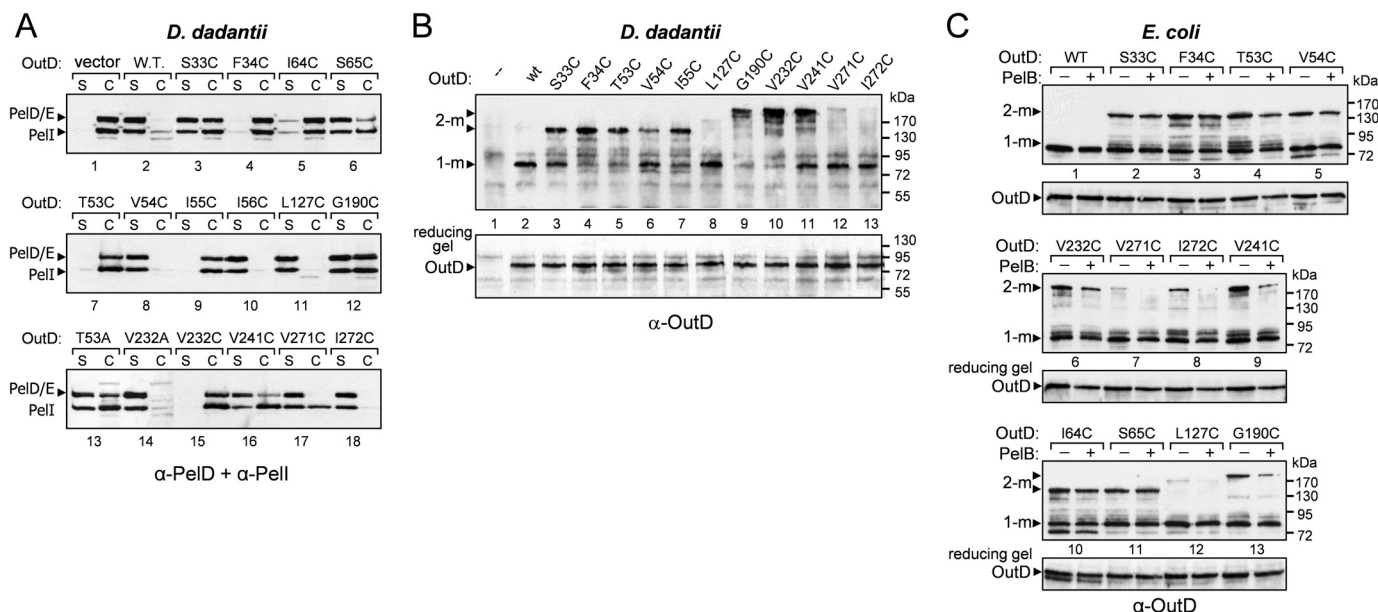


FIGURE 2. Functionality and disulfide bonding patterns of cysteine variants of OutD. *A*, secretion activity of OutD variants. *D. dadantii* A3558 $\Delta outD$ cells, carrying a pTdB-oD plasmid with a mutant *outD* allele (indicated on top), were grown aerobically to steady state, and then the culture supernatant (s) and cells (c) were separated and analyzed by immunoblotting with PelD and PelI antibodies. The quantity of secreted proteins present in the culture supernatant reflects the efficiency of secretion. *B*, disulfide bonding analysis of OutD variants. Cells from the same cultures as in *A* were treated with iodoacetamide, to block any remaining free thiol groups, and the extent of disulfide bonding was assessed using nonreducing SDS-PAGE, followed by immunoblotting with OutD antibodies. To estimate the amounts of OutD loaded onto the gels, the same samples were analyzed in reducing conditions with 2-mercaptoethanol (*lower*). *C*, secreted protein PelB effect on self-bonding of OutD variants: disulfide bonding analysis of the periplasmic domains of OutD. *E. coli* NM522/pACoS (*outS*⁺) cells, carrying a pTdB-oD plasmid with a mutant allele of *outD* and either an empty pACYC184 vector (–) or pACPLB (*pelB*) (+) were grown, treated, and analyzed with OutD antibodies as in *B*. An equivalent amount of cells was loaded into each well. The positions of OutD monomers (1-m) and dimers (2-m) are indicated by arrowheads. The relative amount of homodimer formed by each variant reflects the proximity of the respective residue to the same residue of a neighboring OutD protomer. Note that the homodimers formed by cysteine substitutions close to the protein terminus migrate faster than those located in the middle portion of the protein. Such an altered mobility could result from a different overall shape of these dimers, V-like for the first and X-like for the latter.

Notably, the two other nonfunctional variants, F34C and V232C, also efficiently generated homodimers (Fig. 2*B*, lanes 4 and 10). Supporting the view that the loss of function is due to cross-linking of neighboring domains as opposed to a problem of protein folding, alanine substitutions of Thr-53 and Val-232 were functional (Fig. 2*A*, lanes 13 and 14). A prominent self-cross-linking of certain OutD variants indicates that the corresponding residues are close to the equivalent residues of the neighboring OutD subunit. An explanation for this could be that neighboring N0 domains interact via two distinct sites involving, on the one hand, the $\beta 1^{\text{N0}}$ strand (F34C) and, on the other hand, the $\beta 2^{\text{N0}}$ strand (T53C and I55C) (Fig. 1, *C* and *D*, and supplemental Fig. S1).

When the OutD variants were co-expressed with the pilotin OutS, in *E. coli* cells lacking a T2SS, the respective cross-linking patterns were roughly similar to those in *D. dadantii* (Fig. 2*C*). However, the difference between the solvent-exposed and buried residues was slightly less obvious (compare the extent of dimerization of T53C and V54C in Fig. 2, *B* and *C*). This suggests that in the absence of the functional T2SS, the interdomain contacts of OutD subunits are more flexible and disordered. The recent model suggests that the GspD periplasmic domains form a vestibule where the secretion substrate could be loaded (20, 25). We, therefore, investigated whether the secreted protein PelB affects the extent of self-bonding of OutD. In the presence of PelB, most analyzed variants, except for S33C, F34C, I64C, and S65C, generated a smaller amount of homodimer (Fig. 2*C*). These data suggest that the secreted pro-

tein weakens the mutual proximity of certain sites, implying rearrangements of the periplasmic domains of OutD within the dodecameric complex.

Disulfide Bonding Analysis of HR Domain of OutC—To evaluate the relevance of cysteine substitutions in the HR domain of OutC, corresponding mutant alleles were first expressed from a plasmid in the *D. dadantii* $\Delta outC$ A3556 strain. The abundance of all of the mutants was equivalent to that of the wild-type OutC (Fig. 3*B*, *lower*) and functionality was only lost in G99C ($\beta 1^{\text{HR}}$) (Fig. 3*A*, lane 9). This variant generated a huge amount of homodimer, which appeared in form of three major species (Fig. 3*B*, lane 9). Consistent with the HR structure, cysteine substitutions of the adjacent, but buried, residues Val-100 and Ile-113 produced only a small quantity of homodimer (Figs. 3*B* and 4*B*, lane 3). In contrast, cross-linking of the substitutions located in the second β -sheet (strands $\beta 6^{\text{HR}}$ and $\beta 7^{\text{HR}}$) was inconsistent with the published HR structure. A significant amount of homodimer was generated by the buried L145C and L154C but not the solvent-exposed V144C and V153C (Fig. 3*B*, lanes 5–8). An efficient dimerization of L145C and L154C correlates with a reduced functionality of these variants (Fig. 3*A*, lanes 6 and 8). These data suggest that neighboring HR domains can interact through two opposite sites, one including the solvent-exposed face of the first β -sheet (G99C, $\beta 1^{\text{HR}}$) and the other involving the side chains of Leu-145 and Leu-154 ($\beta 6^{\text{HR}}$ and $\beta 7^{\text{HR}}$, respectively) (supplemental Fig. S2).

It cannot be excluded that unexpected disulfide bonding patterns of the latter OutC variants could be caused by their

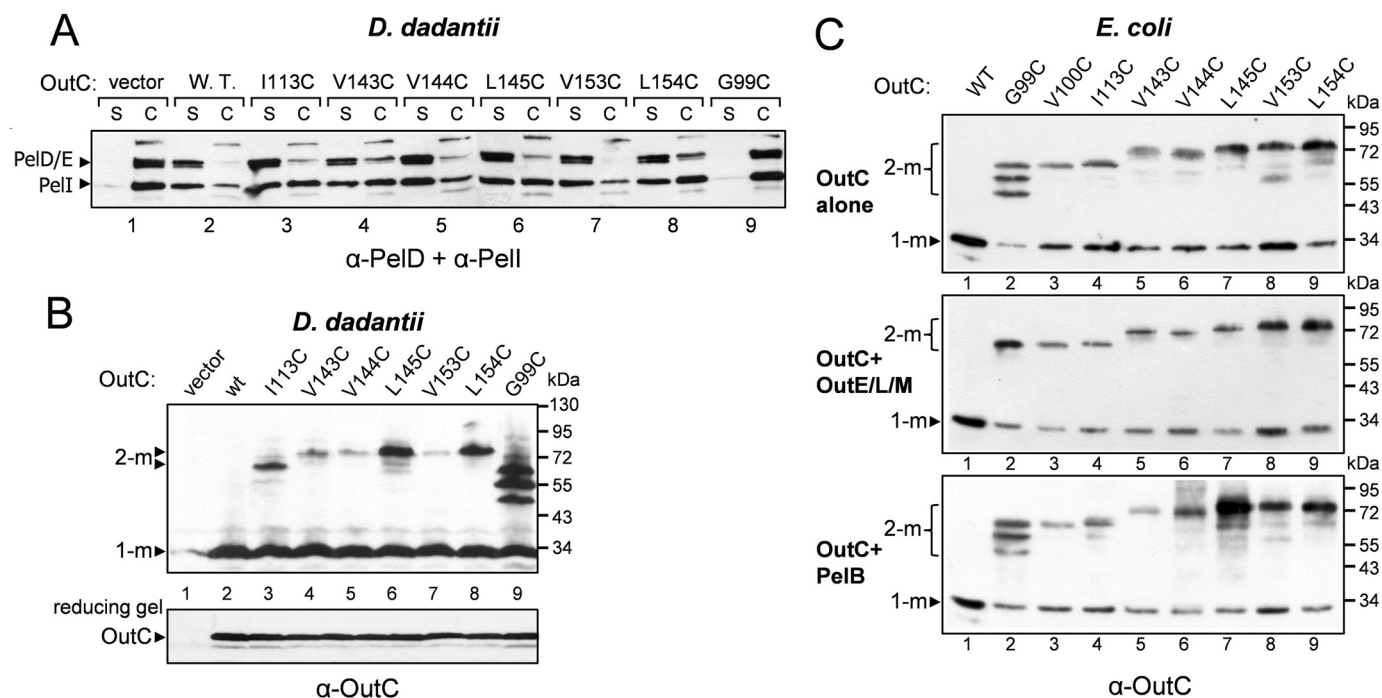


FIGURE 3. Functionality and disulfide bonding patterns of cysteine variants of OutC. *A*, secretion activity of OutC variants. *B*, disulfide bonding analysis of OutC variants. *D. dadantii* A3556 $\Delta outC$ cells, carrying a pTdB-oC plasmid with a mutant *outC* allele (indicated on top) were grown, treated, and analyzed with either PelD and Pell antibodies (*A*) or with OutC antibodies (*B*), as in Fig. 2. The positions of OutC monomers (1-m) and dimers (2-m) are indicated by arrowheads. *C*, secreted protein PelB and the T2SS components OutE/L/M effect on self-bonding of OutC variants. *E. coli* NM522 cells, carrying a pTdB-oC plasmid with a mutant allele of *outC* and either an empty pACYC184 vector (*top*) or pBAD-ELM (*outE/L/M*; *middle*), or pACPLB (*pelB*; *bottom*), were grown and treated as in Fig. 2*B* but with OutC antibodies. The three panels were exposed for different times to ensure an equivalent intensity of the wild-type OutC (*lane 1*). The positions of monomers and dimers are indicated by arrowheads and/or brackets.

expression from plasmids. In this way, mutant *outC* genes, coding for certain cysteine variants, were recombined into the *D. dadantii* chromosome in place of the wild-type allele. The secretion efficiency and disulfide bonding patterns of these mutant strains were similar to those of the corresponding variants expressed from a plasmid (supplemental Fig. S3). Notably, homodimers of OutC were only detected in A5177 and A5212 strains expressing L145C and L154C variants, respectively (supplemental Fig. S3*B*), that supports functional relevance of these self-bondings.

The inner membrane T2SS components, OutL and OutM, and the secretion substrates are thought to interact with OutC (5, 9, 37, 38). To test whether these proteins could influence the arrangement of adjacent HR domains, selected OutC variants were expressed in *E. coli* cells. In comparison with that in *D. dadantii*, a greater quantity of dimers were detected (compare the dimer/monomer ratio in Fig. 3, *B* and *C*) that suggests more disordered interdomain contacts. Nevertheless, the dimer ratio remained most significant with G99C, L145C, and L154C variants (Fig. 3*C*, *top*, lanes 2, 7, and 9). The co-expression of OutE, OutL, and OutM did not significantly affect the cross-linking patterns, except G99C produced a single cross-linking product (Fig. 3*C*, *middle*, lane 2). This suggests that OutE/L/M significantly affect the $\beta 1^{HR}-\beta 1^{HR}$ contact. In contrast, the co-expression of PelB mostly affects the second β -sheet; namely, L145C variant became more abundant and generated a far greater quantity of dimer (Fig. 3*C*, *bottom*, lane 7). Thus, the secreted protein reinforces the $\beta 6^{HR}-\beta 6^{HR}$ contact.

Interface between HR Domain of OutC and N0 domain of OutD Seen in Crystal Structure Is Biologically Relevant—The recent structural studies suppose that the HR/N0 interface involves strand $\beta 1^{HR}$ and may include two different, but adjacent, sites in N0, namely strand $\beta 1^{N0}$ or $\beta 3^{N0}$ (32, 33). To assess the biological relevance of the presumed crystal interface, which includes the $\beta 1^{HR}-\beta 1^{N0}$ contact, the cysteine substitutions in HR (G99C and V100C) were combined pairwise with those in N0 (S33C and F34C), and, subsequently, the cross-linking patterns of respective OutC-OutD pairs were analyzed in *E. coli* and *D. dadantii* $\Delta outC$ and $\Delta outD$ strains. A quantity of the OutC-OutD complex was detected with the OutC^{G99C}-OutD^{F34C} pair but not with the other three combinations (Fig. 4, *A* and *B*, compare lane 6 with 2–5 and 7). These results are consistent with the orientations of the corresponding side chains in the crystal HR/N0 interface and indicate its biological relevance. In contrast, the OutC^{G99C}-OutD^{S65C} couple, which would link the modeled solution structure HR/N0 interface ($\beta 1^{N0}-\beta 3^{N0}$), generated only low amounts of OutC-OutD complex (Fig. 4, *A* and *B*, compare lanes 9 and 10 with 6), suggesting that this interface may not be biologically relevant. However, in all cases, homodimers of the respective OutC and OutD variants were the main cross-linking products (Fig. 4, *B* and *D*), indicating that self-interactions of the HR and N0 domains were much more prevalent than any interaction between these two domains. The functional impact of the OutC^{G99C}-OutD^{F34C} complex remains unclear. Because both OutC^{G99C} and OutD^{F34C} single substitutions were defective in secretion

GspC-GspD Disulfide Bonding Analysis

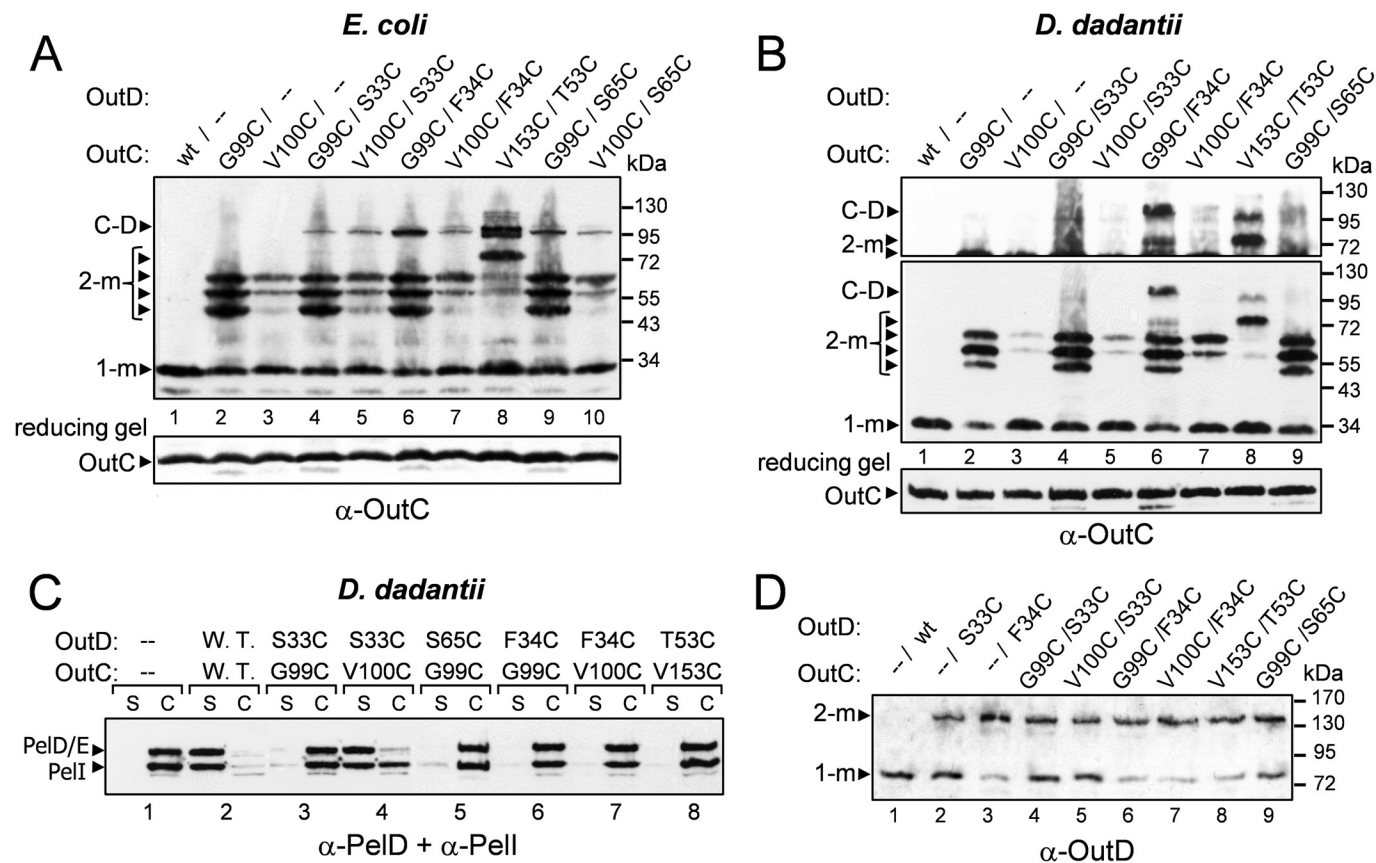


FIGURE 4. Disulfide bonding and functional analysis of the HR-N0 interaction sites deduced from structural studies. *E. coli* NM522/pACoS (*outC*⁺) (A) or *D. dadantii* A3556 Δ *outC* (B and C) or *D. dadantii* A3558 Δ *outD* (D) cells, carrying a pTdB-oCoD plasmid co-expressing mutant alleles of *outC* and *outD* (indicated on top), were grown, treated, and analyzed, as in Fig. 2. The quantity of each OutC variant was estimated from the reducing gel (lower panels). The positions of monomers (1-m), dimers (2-m), and OutC-OutD complexes are indicated by arrowheads. In B, the upper panel was overexposed, compared with the middle panel, to reveal the high molecular mass forms more clearly. Among the combinations of G99C and V100C variants of OutC with S33C, F34C, and S65C variants of OutD, only G99C/F34C provokes an efficient OutC-OutD bonding, both in *E. coli* and *D. dadantii* (A and B, lane 6). A comparable degree of OutC-OutD bonding in the G99C/F34C and V153C/T53C pairs suggests an equivalent biological relevance of the corresponding interactions.

(Figs. 2A and 3A) the OutC-OutD combinations, including one of these variants, were also nonfunctional (Fig. 4C).

Mapping of Two Other OutC-OutD Interaction Sites—Next, the relevance of the OutC-OutD interactions suggested by the previous *in vitro* study (8) was examined. These two presumed interfaces include a short segment of the HR domain, consisting of strands $\beta 6^{\text{HR}}$ and $\beta 7^{\text{HR}}$, and two distinct sites of OutD, located in the N0 and N2-N3 domains, respectively. Therefore, the cysteine substitutions of Val-143, Val-144 ($\beta 6^{\text{HR}}$), Val-153, and Leu-154 ($\beta 7^{\text{HR}}$) in HR were combined pairwise with those in OutD, Thr-53, Val-54, Ile-55, Ile-56 ($\beta 2^{\text{N0}}$), Val-232 ($\beta 10^{\text{N2}}$), Val-241 ($\beta 11^{\text{N2}}$), Val-271, and Ile-272 ($\beta 12^{\text{N3}}$), and then co-expressed in *E. coli*. A quantity of OutC-OutD complex was detected with the OutC^{V153C}-OutD^{T53C} and OutC^{V153C}-OutD^{V232C} pairs, both including the same variant, OutC^{V153C} ($\beta 7^{\text{HR}}$) (Fig. 5, lanes 5 and 13). The nature of these complexes was confirmed by immunoblotting with both OutC and OutD antibodies (supplemental Fig. S4). In contrast, OutC^{V153C} ($\beta 7^{\text{HR}}$) did not form a complex with V241C ($\beta 11^{\text{N2}}$) or V271C ($\beta 12^{\text{N3}}$), indicating that strand $\beta 7^{\text{HR}}$ is proximal to strand $\beta 10^{\text{N2}}$ but not to $\beta 11^{\text{N2}}$ or $\beta 12^{\text{N3}}$ (supplemental Figs. S4 and S5). Conversely, no complex was detected when V144C ($\beta 6^{\text{HR}}$) was used instead of V153C ($\beta 7^{\text{HR}}$), indicating that contrary to strand $\beta 7^{\text{HR}}$, $\beta 6^{\text{HR}}$ is not close to strand $\beta 2^{\text{N0}}$ (T53C) or to

$\beta 10^{\text{N2}}$ (V232C) (Fig. 5, lanes 1 and 9). Consistent with the HR structure, the extent of cross-linking decreased when the buried L154C was used instead of the solvent-exposed V153C (Fig. 6A, lanes 3 and 4). Similarly, consistent with the N0 structure, cysteine substitutions of Thr-53 and Ile-55 (solvent-exposed) but not of Val-54 (buried) gave prominent cross-links with OutC^{V153C} (Fig. 6A, lanes 1–3). To further characterize the mutual orientation of the $\beta 7^{\text{HR}}$ and $\beta 2^{\text{N0}}$ strands, the proximity of Y151C and V153C ($\beta 7^{\text{HR}}$) to T53C and I55C ($\beta 2^{\text{N0}}$) was estimated. The cross-linking patterns suggest that Y151C is closer to T53 than to I55 whereas V153 has a similar proximity to T53 and I55 (Fig. 6A). This is consistent with a parallel arrangement of the two β -strands (Fig. 6B).

Thus, these data suggest the presence of at least three interactions between the HR domain of OutC and the periplasmic domains of OutD, namely (i) OutC^{G99C}-OutD^{F34C} ($\beta 1^{\text{HR}}$ - $\beta 1^{\text{N0}}$), (ii) OutC^{V153C}-OutD^{T53C} ($\beta 7^{\text{HR}}$ - $\beta 2^{\text{N0}}$), and (iii) OutC^{V153C}-OutD^{V232C} ($\beta 7^{\text{HR}}$ - $\beta 10^{\text{N2}}$). More unexpectedly, these results indicate that the same faces of the $\beta 2^{\text{N0}}$ and $\beta 10^{\text{N2}}$ strands (Thr-53 and Val-232) could control the self-interaction of OutD subunits and their interactions with HR.

Secreted Proteins and Inner Membrane Components of T2SS Have Different Effects on OutC-OutD Interacting Sites—To investigate whether the secreted proteins could influence

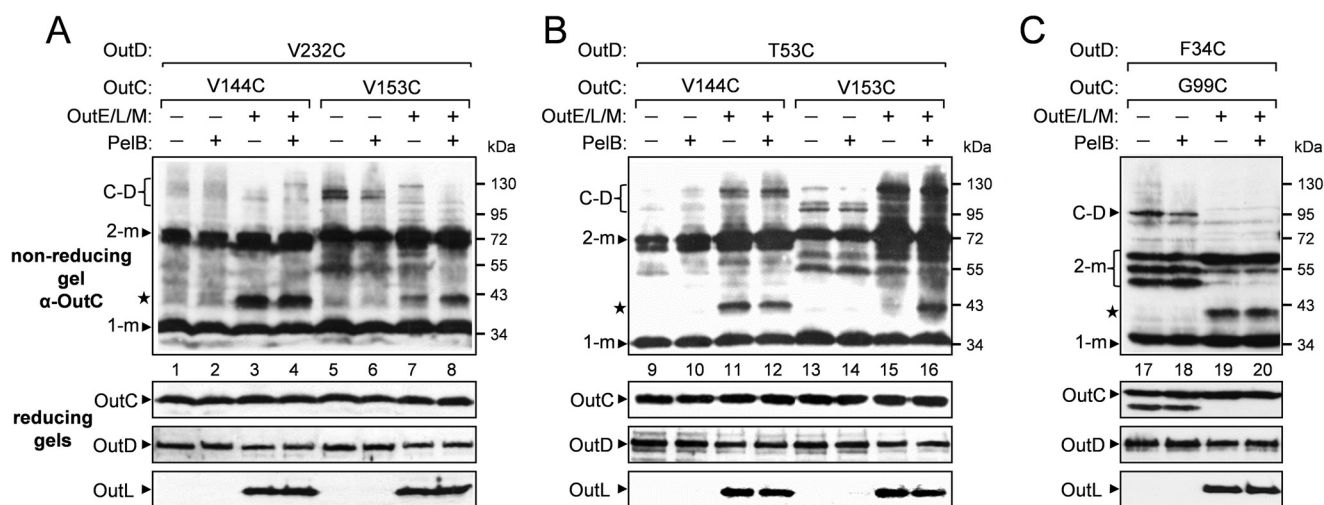


FIGURE 5. Secreted protein PelB and the T2SS components OutE/L/M affect disulfide bonding efficiency between various OutC and OutD variants differently. *E. coli* NM522/pACoS (*outs*⁺) cells carrying either a pTdB-oCoD (*pelB*⁻) or a pTPLB-oCoD (*pelB*⁺) plasmid, co-expressing the mutant alleles of *outC* and *outD* (indicated on top) and either an empty pBAD18 vector or pBAD-ELM (*outE/L/M*⁺), were grown, treated, and analyzed with OutC antibodies, as in Fig. 2B (upper panels). All samples were equilibrated to load an equivalent amount of each OutC variant, as estimated from gels in reducing conditions (lower panels). The monomers (1-m) and dimers (2-m) of OutC are indicated by arrowheads, and OutC-OutD complexes are indicated by brackets. An uncharacterized OutC adduct is indicated by an asterisk. The extent of disulfide bonding between OutC and OutD (upper panels) suggests that the same position of OutC (V153C, $\beta 7^{\text{HR}}$) is close to two distant positions of OutD, V232C ($\beta 10^{\text{N0}}$) (A) and T53C ($\beta 2^{\text{N0}}$) (B). When *outE/L/M* are also co-expressed, the amount of the OutC-OutD complex in A and C decreased but increased in B. Co-expression of *outE/L/M* provokes a more efficient homodimerization of both OutC variants (2-m), together with the appearance of an uncharacterized OutC adduct (indicated by an asterisk).

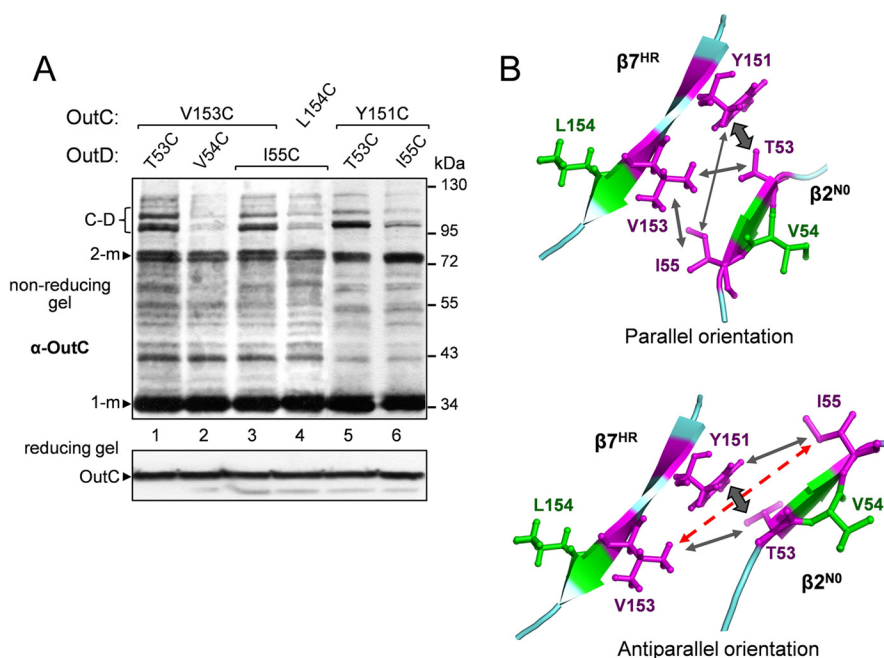


FIGURE 6. Analysis of the relative orientation of strands $\beta 7$ of HR and $\beta 2$ of N0 using disulfide bonding. A, *E. coli* NM522 cells carrying pACoS (*outs*⁺) and pTdB-oCoD plasmids, co-expressing mutant alleles of *outC* and *outD* (indicated on top), were grown, treated, and analyzed with OutC antibodies, as in Fig. 2B. All samples were equilibrated to load an equivalent amount of each OutC variant, as estimated from gels in reducing conditions (lower panels). The positions of OutC monomers (1-m), dimers (2-m), and OutC-OutD complexes are indicated by arrowheads and brackets, respectively. The extent of disulfide bonding suggests that Tyr-151 is closer to Thr-53 than to Ile-55, whereas Val-153 has the same proximity to both Thr-53 and Ile-55. B, two presumed modes of relative orientation of the $\beta 7^{\text{HR}}$ and $\beta 2^{\text{N0}}$ strands are shown. The solvent-exposed side chains are shown in magenta, and the buried ones are in green. Width of arrows reflects the proximity between the various residues. The parallel arrangement of these β -strands is compatible with the extent of disulfide bonding in A.

the OutC-OutD interactions, combinations of OutC-OutD variants were systematically co-expressed, either alone or together with the pectate lyase PelB, in *E. coli*. In the presence of PelB, the extent of cross-linking with the OutC^{G99C}-OutD^{F34C} and OutC^{V153C}-OutD^{V232C} pairs, representative of the first ($\beta 1^{\text{HR}}-\beta 1^{\text{N0}}$) and the third ($\beta 7^{\text{HR}}-\beta 10^{\text{N2}}$) inter-

acting sites, respectively, diminished (Fig. 5, A and C, lanes 5, 6, 17, and 18). In contrast, PelB did not have any obvious effect on the OutC^{V153C}-OutD^{T53C} couple, representative of the second interacting site ($\beta 7^{\text{HR}}-\beta 2^{\text{N0}}$) (Fig. 5B, lanes 13 and 14). Thus, it seems likely that the secreted substrate has a different effect on the interactions of strand $\beta 7^{\text{HR}}$ with

GspC-GspD Disulfide Bonding Analysis

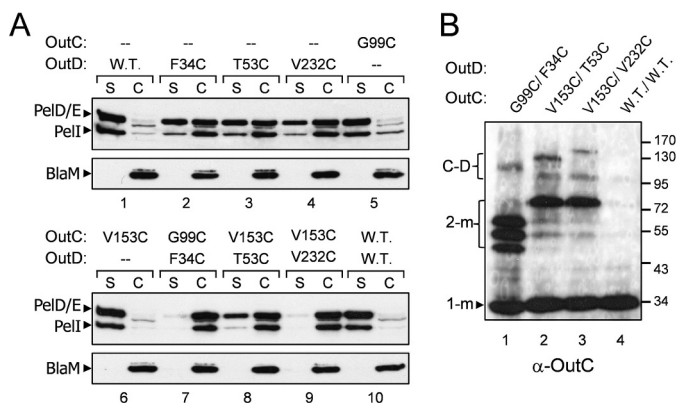


FIGURE 7. Cysteine variants of OutC and OutD interfere differently with pectinase secretion. *D. dadantii* wild-type strain was transformed with a plasmid expressing various alleles of *outC* and *outD* (indicated on top). The bacteria were grown, treated, and analyzed with either PelD and Pell antibodies (A) or with OutC antibodies (B), as in Fig. 2. The amount of secreted proteins (PelD, PelE, and Pell) in the culture supernatant reflects the efficiency of secretion. A, positions of OutC monomers (1-m), dimers (2-m), and OutC-OutD complexes are indicated by arrowheads and brackets.

strands $\beta 10^{N2}$ and $\beta 2^{N0}$ (Fig. 5, compare lanes 5 and 6 with 13 and 14).

Co-expression of OutE, OutL, and OutM with OutC-OutD pairs, in *E. coli* cells, provoked a significant increase in the quantity of OutC but not of OutD, and so the ratio of OutC increased in the presence of OutE/L/M. (supplemental Fig. S5). Because to assess the cross-linking between OutC and OutD, an equivalent amount of OutC was systematically loaded onto the nonreducing gels, the samples with OutE/L/M contained a slightly smaller amount of OutD (Fig. 5, reducing gel panels). Despite this, in the presence of OutE/L/M, the extent of cross-linking with the OutC^{V153C}-OutD^{T53C} pair ($\beta 7^{HR}$ - $\beta 2^{N0}$ site) was obviously increased (Fig. 5B, compare lanes 13 and 15). Remarkably, the largest cross-linked species (apparent mass of 120 kDa) became very abundant, suggesting that OutE/L/M enhanced this OutC-OutD interaction and/or improved stability of the complex. In contrast, OutE/L/M generated an opposite effect on the other two OutC-OutD interacting sites and the level of cross-linking with OutC^{V153C}-OutD^{V232C} ($\beta 7^{HR}$ - $\beta 10^{N2}$) and OutC^{G99C}-OutD^{F34C} ($\beta 1^{HR}$ - $\beta 1^{N0}$) decreased significantly (Fig. 5, A and C compare lanes 5 with 7 and 17 with 19). Thus, the secreted proteins and OutE/L/M components differently affect on the tested OutC-OutD interactions.

Various OutC and OutD Variants Interfere Differently with Functional T2SS of *D. dadantii*—Certain OutC (G99C) and OutD (F34C, T53C, and V232C) variants efficiently formed homo- and heterodimers and were fully nonfunctional when expressed in $\Delta outC$ or $\Delta outD$ *D. dadantii* strains (Figs. 2–4). At least in the case of T53C and V232C, dimerization likely is the direct cause of the loss of function (Fig. 2A). To estimate the interference of the cross-linked complexes with the functional T2SS, these variants were expressed in the wild-type *D. dadantii*. The three tested OutD variants significantly impaired secretion (Fig. 7A, lanes 2–4), indicating that they are integrated in the T2SS and compete efficiently with the wild-type OutD. In contrast, OutCG99C did not produce any negative trans-dominant effect, suggesting that this variant does not compete with the wild-type OutC. Co-expression of the vari-

ants, representative of the three interaction sites, produced variable effects. Secretion was fully arrested with the OutC^{G99C}-OutD^{F34C} and OutC^{V153C}-OutD^{V232C} pairs but partially retained with OutC^{V153C}-OutD^{T53C} (Fig. 7A, lanes 7–9). Thus, it seems likely that the two former complexes, even if produced at a small quantity (Fig. 7B), interfere very efficiently with the functional T2SS and completely block it. In contrast, the OutC^{V153C}-OutD^{T53C} complex seems to be unable to interfere with the secretion system.

DISCUSSION

We have used cysteine scanning and disulfide bonding analysis to study the organization of OutC and OutD subunits in the T2S machinery and the interactions between these components. Although this analysis is not comprehensive, it does reveal some important features of the assembly of this secretion machinery. The disulfide bonding assays suggest the presence of at least three distinct sites of interactions between the periplasmic domains of OutC and OutD, namely 1) $\beta 1^{HR}$ - $\beta 1^{N0}$, 2) $\beta 7^{HR}$ - $\beta 2^{N0}$, and 3) $\beta 7^{HR}$ - $\beta 10^{N2}$ (supplemental Fig. S6). Interfaces 2 and 3 were already suggested in our previous study (8), and the first is consistent with the recently established crystal structure of the HR/N0-N1 complex (32). In contrast, disulfide bonding analysis suggested that the HR/N0 interface, detected in our recent NMR study ($\beta 1^{HR}$ - $\beta 3^{N0}$), is much less prevalent *in vivo* (33). However, it is also possible that an optimal arrangement of the cysteine substitutions has not been achieved in the latter case. Moreover, it should be noted that in the corresponding crystal and solution structures, the HR/N0 interface involves the same $\beta 1^{HR}$ -strand of HR but two different, though adjacent, β -strands of N0, $\beta 1^{N0}$, and $\beta 3^{N0}$, respectively. This apparent discrepancy could result from the varied composition of the OutD derivatives used in these studies, the N0-N1 domains and the isolated N0 domain, respectively (32, 33). Indeed, in the N0-N1 derivative, strand $\beta 3^{N0}$, is involved in the N0/N1 interface and interacts with $\beta 6^{N1}$ (26, 32), and consequently, it is not well accessible for an interaction with HR. Alternatively, the different affinities of N0 for HR in the *Vibrio cholerae* and *D. dadantii* proteins could be the origin of the discrepancy. Finally, dissimilar experimental approaches used in different studies can also contribute to the data conflict. Indeed, this report and the previous pulldown analysis (8) indicate an HR-N2 interaction ($\beta 7^{HR}$ - $\beta 10^{N2}$); however, the recent NMR analysis (33) did not reveal any interaction of the HR domain with the isolated N1-N2 domains. Similarly, the recent systematic surface plasmon resonance analysis of the T2SS of *Pseudomonas aeruginosa* has indicated that the periplasmic region of GspC interacts with N3 but not with N0 domain of the cognate secretin (10). Once again, particular experimental approaches employed in this study (surface plasmon resonance and affinity chromatography) could be the cause. Alternatively, because the *P. aeruginosa* GspC and GspD is much more dissimilar from those of *D. dadantii* and *E. coli*, the observed discrepancies could reflect some subtle mechanistic differences between these T2SSs.

The OutC-OutD interactions, 2) $\beta 7^{HR}$ - $\beta 2^{N0}$ and 3) $\beta 7^{HR}$ - $\beta 10^{N2}$, involve the same site of HR ($\beta 7^{HR}$) and, hence, seem to be mutually incompatible (supplemental Fig. S6). In contrast,

interaction 1), $\beta 1^{\text{HR}}-\beta 1^{\text{N0}}$, seems to be compatible with the two others because it involves distinct sites of HR and N0 (supplemental Fig. S6, B and C). However, in the GspD crystal structure, $\beta 1^{\text{N0}}$ and $\beta 10^{\text{N2}}$ are far apart (Fig. 1D). Thus, even if steric constraints would allow a simultaneous interaction of HR with these two sites of OutD, this would necessitate substantial rearrangements of the periplasmic domains of OutD (supplemental Fig. S6B). Interactions 1) and 2) involve two opposite faces of the HR domain ($\beta 1^{\text{HR}}$ and $\beta 7^{\text{HR}}$) and two distinct sites of the N0 domain ($\beta 1^{\text{N0}}$ and $\beta 2^{\text{N0}}$) and, hence, they look spatially compatible with each other (supplemental Fig. S6C, left). However, the inner membrane components, OutE/L/M, have opposite effects on these interactions, reinforcing 2) but reducing 1) (supplemental Fig. S6C, right). Therefore, the three OutC-OutD interactions are not at all, or only poorly, compatible simultaneously, and this implies an alternation of their activity during the process of secretion.

In addition, the transient nature of various OutC-OutD interactions is suggested by the fact that the same sites of these proteins are also involved in self-interactions. For example, both OutC^{G99C} ($\beta 1^{\text{HR}}$) and OutD^{F34C} ($\beta 1^{\text{N0}}$) produce homodimers when expressed separately but, once combined, they create a heterodimer. Similarly, both OutD^{T53C} ($\beta 2^{\text{N0}}$) and OutD^{V232C} ($\beta 10^{\text{N2}}$) self-interact but also interact with OutC^{V153C} ($\beta 7^{\text{HR}}$). Thus, none of these interactions occurs through static interfaces. It is striking that disulfide self-bonding at positions involved in multiple interactions abolishes the protein function, e.g. OutD variants F34C, T53C, and V232C were all shown to be completely defective for secretion. In contrast, some OutD variants, which have not been shown to interact with OutC, are dimeric but remain functional (e.g. G190C and V241C), indicating that homodimerization of OutD *per se* may be compatible with the protein function.

Equivalent amounts of OutC-OutD complexes were observed with the three interacting sites, suggesting that they have a similar functional relevance. It seems, however, symptomatic that the extent of OutC-OutD cross-linking was rather low compared with that of self-bonding of the corresponding OutC and OutD variants. This suggests that self-interactions of HR and N0-N3 domains are more prevalent and could constitute the initial or "basal" interactions within the secretin, whereas heterogeneous contacts between these domains are transient and loose. Indeed, efficiency of disulfide cross-linking is dependent on the proximity and proper orientation of the sites studied but also on the prevalence of these contacts. Thus, the interactions representative of the "stand-by" state of the system would generate more efficient cross-linking than the transient, but functionally important, contacts.

Experiments with *E. coli* demonstrated that the equilibrium between various homo- and heterogeneous interactions could be altered by the presence of the secreted substrate and/or the inner membrane components. Co-expression of PelB with certain variants of OutC or OutD provoked effects suggesting direct interactions of the secreted substrate with these components and so, indicating some individual sites that are particularly affected by the secreted protein. More precisely, the quantity of homodimers and/or the total amount of OutD decreased significantly with T53C, G190C, V232C, V241C, and I272C

variants indicating that, in these positions, self-interactions between subunits of OutD are poorly compatible with the presence of PelB. The three-dimensional reconstruction of the GspD dodecameric complex assumes that the ring-like structures, formed by the N1 and N2 domains, constitute a vestibule in which the secretion substrate is loaded prior to being secreted, whereas the N3 domain builds up a form of constriction which closes the pore (20, 25). Thus, it seems reasonable that the secreted protein PelB affects multiple sites of the secretin. Remarkably, in the N0 domain, PelB apparently affects only one of the two self-interacting sites (supplemental Fig. S1C). This site, involving strand $\beta 2$ (Thr-53), could indicate a point of entry of the secretion substrate.

In addition, PelB provokes a striking effect on certain OutC variants, namely, it increases the self-bonding of L145C (supplemental Fig. S2C). This suggests that some local unfolding or β -strand switching occurs; i.e. PelB causes $\beta 6^{\text{HR}}$ strand to move out in the way that Leu-145 (buried in the HR structure) became accessible for disulfide cross-linking. This self-interaction was also observed in *D. dadantii*, and hence, it could indicate mode of interaction of the secreted substrate with HR. Indeed, the recent surface plasmon resonance analysis showed that the periplasmic region of the *P. aeruginosa* GspC interacts with the secreted substrate (10). Alternatively, it cannot be completely excluded that substitution of the hydrophobic Leu by nucleophilic Cys affects hydrophobic core of the HR domain and provokes such a behavior. However, analysis of the double and triple cysteine substitutions in HR shows that even multiple cysteine substitutions *per se* are well compatible with OutC function and, thus, do not affect drastically the folding of HR (supplemental text and supplemental Fig. S7).

The T2SS components OutE/L/M produce another significant effect on OutC, as they improve its dimerization via the $\beta 1^{\text{HR}}/\beta 1^{\text{HR}}$ (G99C) interface (supplemental Fig. S2C). Indeed, G99C generated three species on nonreducing gel, whereas the protein itself was not degraded (Fig. 3B). Because electrophoretic mobility of dimers dependent on their overall shape (see Fig. 2 legend), these species may correspond to three different conformations. In fact, Gly-99 is located on a tight bend of $\beta 1^{\text{HR}}$, and G99C mutant may have two conformations, named A and B. Next, they can generate AA, BB, AB, and BA dimers, where the two latter have the same shape. If this suggestion is true, the presence of OutE/L/M imposes only one conformation of G99C and, thus, only one type of dimers.

Certain other disulfide bonding patterns seem to be poorly consistent with the structural data; namely, both $\beta 1^{\text{N0}}-\beta 1^{\text{N0}}$ and $\beta 1^{\text{N0}}-\beta 1^{\text{HR}}$ interactions involve Phe-34. This residue, however, appears as buried on the OutD model (Fig. 1D) and on the structure of isolated N0-N1-N2 domains from ETEC, which has been used as a template (Phe-34 corresponds to Phe-9 on PDB 3EZJ) (26). On the other hand, in the structure of the HR/N0-N1 complex from ETEC (PDB 3OSS) (32), $\beta 1^{\text{N0}}$ forms a mixed β -sheet with $\beta 1^{\text{HR}}$ at the manner that the side chain of Phe-9 (Phe-34) is involved in the HR/N0 interface. Thus, the latter study shows that apparently buried Phe-34 remains accessible and suggests a way by which the side chains of two Phe-34 residues can interact in the $\beta 1^{\text{N0}}-\beta 1^{\text{N0}}$ interface presumed by disulfide bonding assays. This example can also illus-

GspC-GspD Disulfide Bonding Analysis

trate how some other buried residues, namely, L145C and L154C variants of OutC, may be involved in interdomain contacts.

Another rather unexpected observation may be drawn from this cysteine bonding analysis. Notably, homodimers were predominant with several of the OutD variants, both in *E. coli* and in *D. dadantii*. Such efficient self-bonding could not be straightforwardly attributed to the sporadic movements of the periplasmic domains of OutD because no dimers were observed with some variants (L127C and V271C), and cysteine substitutions of buried side chains generated significantly less homodimers than those of adjacent, but solvent-exposed, residues (e.g. V54C and I56C versus T53C and I55C). An efficient self-cross-linking of certain OutD variants indicates that the corresponding residues are close to the same residues of an adjacent OutD protomer (e.g. Phe-34 to Phe-34, Thr-53 to Thr-53, Val-232 to Val-232, etc.) and also suggests a juxtaposition of the corresponding structural elements ($\beta 1$ to $\beta 1$, $\beta 2$ to $\beta 2$, $\beta 10$ to $\beta 10$, etc.) (supplemental Fig. S1). Such an arrangement of adjacent OutD domains is poorly compatible with C12 rotational symmetry suggested for the GspD dodecamer (20, 26), which implies the same arrangement of each OutD subunit. In the latter case, the distance between the equivalent side chains and their mutual orientation would not allow for an efficient self-bonding of OutD. Our data therefore suggest an alternative organization of the OutD subunits. The equivalent periplasmic domains of two adjacent OutD protomers may be arranged with 2-fold symmetry to allow for proximity and the appropriate orientation of the equivalent structural elements. Similarly, cysteine bonding analysis of the HR domain suggests a juxtaposition of two neighboring OutC protomers, either via the $\beta 1$ - $\beta 1$ self-interaction (G99C) or via substrate-induced contacts of strands $\beta 6$ and $\beta 7$ (L145C and L154C, respectively) (supplemental Fig. S1B). Once again, a 2-fold arrangement of each pair of OutC subunits would account for the observed disulfide-linked species. Interestingly, initially the GspE hexamer was also modeled with P6 symmetry, assuming the same conformation for each GspE subunit (39). However, based on the recent structural data on PilT, a GspE ortholog from the T4P (40), a C2 hexameric model of GspE was generated which involves three different conformations of the GspE subunits (41). It is, therefore, plausible that the GspD and GspC subunits could also have different conformations within the secreton, compatible with a high level of disulfide self-bonding of various cysteine variants. Consequently, the periplasmic domains of the GspD dodecamer may be arranged as a hexamer of dimers (6-fold rotational symmetry) rather than a dodecamer with 12-fold rotational symmetry (supplemental Fig. S1A). The same arrangement might extend to the GspC subunits. Moreover, considering the transient nature of many of the interactions, elucidated in this study, such conformations could also be transient, varying according to the interactions with other T2SS components and/or secreted proteins.

Acknowledgments—We are grateful to Beatrice Py for the OutE/L/M plasmid, to Xavier Robert, for OutD modeling, and to Guy Condemine, for reading the manuscript.

REFERENCES

1. Filloux, A. (2004) The underlying mechanisms of type II protein secretion. *Biochim. Biophys. Acta* **1694**, 163–179
2. Cianciotto, N. P. (2005) Type II secretion: a protein secretion system for all seasons. *Trends Microbiol.* **13**, 581–588
3. Py, B., Loiseau, L., and Barras, F. (2001) An inner membrane platform in the type II secretion machinery of Gram-negative bacteria. *EMBO Rep.* **2**, 244–248
4. Tsai, R. T., Leu, W. M., Chen, L. Y., and Hu, N. (2002) A reversibly dissociable ternary complex formed by XpsL, XpsM, and XpsN of the *Xanthomonas campestris* pv. *campestris* type II secretion apparatus. *Biochem. J.* **367**, 865–871
5. Lee, H. M., Chen, J. R., Lee, H. L., Leu, W. M., Chen, L. Y., and Hu, N. T. (2004) Functional dissection of the XpsN (GspC) protein of the *Xanthomonas campestris* pv. *campestris* type II secretion machinery. *J. Bacteriol.* **186**, 2946–2955
6. Robert, V., Filloux, A., and Michel, G. P. (2005) Subcomplexes from the Xcp secretion system of *Pseudomonas aeruginosa*. *FEMS Microbiol. Lett.* **252**, 43–50
7. Korotkov, K. V., Krumm, B., Bagdasarian, M., and Hol, W. G. (2006) Structural and functional studies of EpsC, a crucial component of the type 2 secretion system from *Vibrio cholerae*. *J. Mol. Biol.* **363**, 311–321
8. Login, F. H., Fries, M., Wang, X., Pickersgill, R. W., and Shevchik, V. E. (2010) A 20-residue peptide of the inner membrane protein OutC mediates interaction with two distinct sites of the outer membrane secretin OutD and is essential for the functional type II secretion system in *Erwinia chrysanthemi*. *Mol. Microbiol.* **76**, 944–955
9. Bouley, J., Condemine, G., and Shevchik, V. E. (2001) The PDZ domain of OutC and the N-terminal region of OutD determine the secretion specificity of the type II out pathway of *Erwinia chrysanthemi*. *J. Mol. Biol.* **308**, 205–219
10. Douzi, B., Ball, G., Cambillau, C., Tegoni, M., and Voulhoux, R. (2011) Deciphering the Xcp *Pseudomonas aeruginosa* type II secretion machinery through multiple interactions with substrates. *J. Biol. Chem.* **286**, 40792–40801
11. Johnson, T. L., Abendroth, J., Hol, W. G., and Sandkvist, M. (2006) Type II secretion: from structure to function. *FEMS Microbiol. Lett.* **255**, 175–186
12. Hardie, K. R., Lory, S., and Pugsley, A. P. (1996) Insertion of an outer membrane protein in *Escherichia coli* requires a chaperone-like protein. *EMBO J.* **15**, 978–988
13. Shevchik, V. E., and Condemine, G. (1998) Functional characterization of the *Erwinia chrysanthemi* OutS protein, an element of a type II secretion system. *Microbiology* **144**, 3219–3228
14. Gu, S., Rehman, S., Wang, X., Shevchik, V. E., and Pickersgill, R. W. (2012) Structural and functional insights into the pilotin-secretin complex of the type II secretion system. *PLoS Pathog.* **8**, e1002531
15. Opalka, N., Beckmann, R., Boisset, N., Simon, M. N., Russel, M., and Darst, S. A. (2003) Structure of the filamentous phage pIV multimer by cryoelectron microscopy. *J. Mol. Biol.* **325**, 461–470
16. Hodgkinson, J. L., Horsley, A., Stabat, D., Simon, M., Johnson, S., da Fonseca, P. C., Morris, E. P., Wall, J. S., Lea, S. M., and Blocker, A. J. (2009) Three-dimensional reconstruction of the *Shigella* T3SS transmembrane regions reveals 12-fold symmetry and novel features throughout. *Nat. Struct. Mol. Biol.* **16**, 477–485
17. Burkhardt, J., Vonck, J., and Averhoff, B. (2011) Structure and function of PilQ, a secretin of the DNA transporter from the thermophilic bacterium *Thermus thermophilus* HB27. *J. Biol. Chem.* **286**, 9977–9984
18. Korotkov, K. V., Gonen, T., and Hol, W. G. (2011) Secretins: dynamic channels for protein transport across membranes. *Trends Biochem. Sci.* **36**, 433–443
19. Collins, R. F., Frye, S. A., Kitmitto, A., Ford, R. C., Tønjum, T., and Derrick, J. P. (2004) Structure of the *Neisseria meningitidis* outer membrane PilQ secretin complex at 12 Å resolution. *J. Biol. Chem.* **279**, 39750–39756
20. Reichow, S. L., Korotkov, K. V., Hol, W. G., and Gonen, T. (2010) Structure of the cholera toxin secretion channel in its closed state. *Nat. Struct. Mol. Biol.* **17**, 1226–1232
21. Jain, S., Mościcka, K. B., Bos, M. P., Pachulec, E., Stuart, M. C., Keegstra,

- W., Boekema, E. J., and van der Does, C. (2011) Structural characterization of outer membrane components of the type IV pili system in pathogenic *Neisseria*. *PLoS One* **6**, e16624
22. Nouwen, N., Stahlberg, H., Pugsley, A. P., and Engel, A. (2000) Domain structure of secretin PulD revealed by limited proteolysis and electron microscopy. *EMBO J.* **19**, 2229–2236
 23. Chami, M., Guilvout, I., Gregorini, M., Rémy, H. W., Müller, S. A., Valerio, M., Engel, A., Pugsley, A. P., and Bayan, N. (2005) Structural insights into the secretin PulD and its trypsin-resistant core. *J. Biol. Chem.* **280**, 37732–37741
 24. Shevchik, V. E., Robert-Baudouy, J., and Condemine, G. (1997) Specific interaction between OutD, an *Erwinia chrysanthemi* outer membrane protein of the general secretory pathway, and secreted proteins. *EMBO J.* **16**, 3007–3016
 25. Reichow, S. L., Korotkov, K. V., Gonen, M., Sun, J., Delarosa, J. R., Hol, W. G., and Gonen, T. (2011) The binding of cholera toxin to the periplasmic vestibule of the type II secretion channel. *Channels* **5**, 215–218
 26. Korotkov, K. V., Pardon, E., Steyaert, J., and Hol, W. G. (2009) Crystal structure of the N-terminal domain of the secretin GspD from ETEC determined with the assistance of a nanobody. *Structure* **17**, 255–265
 27. Kanamaru, S., Leiman, P. G., Kostyuchenko, V. A., Chipman, P. R., Mesyanzhinov, V. V., Arisaka, F., and Rossmann, M. G. (2002) Structure of the cell-puncturing device of bacteriophage T4. *Nature* **415**, 553–557
 28. Yip, C. K., Kimbrough, T. G., Felise, H. B., Vuckovic, M., Thomas, N. A., Pfuetzner, R. A., Frey, E. A., Finlay, B. B., Miller, S. I., and Strynadka, N. C. (2005) Structural characterization of the molecular platform for type III secretion system assembly. *Nature* **435**, 702–707
 29. Thomas, J. D., Reeves, P. J., and Salmond, G. P. (1997) The general secretion pathway of *Erwinia carotovora* subsp. *carotovora*: analysis of the membrane topology of OutC and OutF. *Microbiology* **143**, 713–720
 30. Peabody, C. R., Chung, Y. J., Yen, M. R., Vidal-Ingigliardi, D., Pugsley, A. P., and Saier, M. H. (2003) Type II protein secretion and its relationship to bacterial type IV pili and archaeal flagella. *Microbiology* **149**, 3051–3072
 31. Login, F. H., and Shevchik, V. E. (2006) The single transmembrane segment drives self-assembly of OutC and the formation of a functional type II secretion system in *Erwinia chrysanthemi*. *J. Biol. Chem.* **281**, 33152–33162
 32. Korotkov, K. V., Johnson, T. L., Jobling, M. G., Pruneda, J., Pardon, E., Héroux, A., Turley, S., Steyaert, J., Holmes, R. K., Sandkvist, M., and Hol, W. G. (2011) Structural and functional studies on the interaction of GspC and GspD in the type II secretion system. *PLoS Pathog.* **7**, e1002228
 33. Gu, S., Kelly, G., Wang, X., Frenkiel, T., Shevchik, V. E., and Pickersgill, R. W. (2012) Solution structure of homology region (HR) domain of type II secretion system. *J. Biol. Chem.* **287**, 9072–9080
 34. Eswar, N., Webb, B., Marti-Renom, M. A., Madhusudhan, M. S., Eramian, D., Shen, M. Y., Pieper, U., and Sali, A. (2007) Comparative protein structure using MODELLER. *Curr. Protoc. Protein Sci.* Chapter 2, Unit 2.9
 35. Laskowski, R. A., MacArthur, M. W., Moss, D. S., and Thornton, J. M. (1993) PROCHECK: a program to check the stereochemical quality of protein structures. *J. Appl. Crystallogr.* **26**, 283–291
 36. Remaut, H., and Waksman, G. (2006) Protein-protein interaction through β -strand addition. *Trends Biochem. Sci.* **31**, 436–444
 37. Possot, O. M., Vignon, G., Bomchil, N., Ebel, F., and Pugsley, A. P. (2000) Multiple interactions between pullulanase secretion components involved in stabilization and cytoplasmic membrane association of PulE. *J. Bacteriol.* **182**, 2142–2152
 38. Gérard-Vincent, M., Robert, V., Ball, G., Blevès, S., Michel, G. P., Lazdunski, A., and Filloux, A. (2002) Identification of XcpP domains that confer functionality and specificity to the *Pseudomonas aeruginosa* type II secretion apparatus. *Mol. Microbiol.* **44**, 1651–1665
 39. Robien, M. A., Krumm, B. E., Sandkvist, M., and Hol, W. G. (2003) Crystal structure of the extracellular protein secretion NTPase EpsE of *Vibrio cholerae*. *J. Mol. Biol.* **333**, 657–674
 40. Misić, A. M., Satyshur, K. A., and Forest, K. T. (2010) *P. aeruginosa* PilT structures with and without nucleotide reveal a dynamic type IV pilus retraction motor. *J. Mol. Biol.* **400**, 1011–1021
 41. Patrick, M., Korotkov, K. V., Hol, W. G., and Sandkvist, M. (2011) Oligomerization of EpsE coordinates residues from multiple subunits to facilitate ATPase activity. *J. Biol. Chem.* **286**, 10378–10386
 42. Hugouvieux-Cotte-Pattat, N., and Charaoui-Boukerzaza, S. (2009) Catabolism of raffinose, sucrose, and melibiose in *Erwinia chrysanthemi* 3937. *J. Bacteriol.* **191**, 6960–6967
 43. Dykxhoorn, D. M., St Pierre, R., and Linn, T. (1996) A set of compatible tac promoter expression vectors. *Gene* **177**, 133–136
 44. Chang, A. C., and Cohen, S. N. (1978) Construction and characterization of amplifiable multicopy DNA cloning vehicles derived from the P15A cryptic miniplasmid. *J. Bacteriol.* **134**, 1141–1156
 45. Py, B., Loiseau, L., and Barras, F. (1999) Assembly of the type II secretion machinery of *Erwinia chrysanthemi*: direct interaction and associated conformational change between OutE, the putative ATP-binding component and the membrane protein OutL. *J. Mol. Biol.* **289**, 659–670